ORIGINAL RESEARCH

Label-Free Electrochemical Immunosensor Based on Gold and Iron-Oxide Nanoparticle Co-modified rGO-TEPA Hybrid for Sensitive Detection of Carcinoembryonic Antigen

Haolin Xiao[1] · Shanshan Wei[1,2] · Zhencheng Chen[1] · Liangli Cao[2,3]

Abstract

Herein we report a label-free amperometric immunosensor based on reduced graphene oxide-tetraethylene pentamine (rGO-TEPA) hybrid material co-modified by gold and iron-oxide magnetic nanoparticles (Au/MNPs-rGO-TEPA) for detection of carcinoembryonic antigen (CEA). The Au/MNPs-rGO-TEPA nanomaterials were prepared and coated on the working electrode as a sensing platform for antibody (anti-CEA) immobilization and signal amplification. This nanomaterial exhibited some excellent functionalities, such as magnetic and enhanced electrical properties due to its large specific surface area and favorable conductivity. Thionine (Thi) molecule was attached onto rGO-TEPA via π-π stacking and was used as an electrochemically active substance. The immunosensor was developed based on the increase in quantity of CEA captured, proportional to the decrease in peak currents of Thi. Under optimal conditions, the Au/MNPs-rGO-TEPA/Thi-based immunosensor showed impressive linear range from 0.1 pg/mL to 150 ng/mL. In addition, the proposed method had excellent linearity, high sensitivity, and relatively good stability, thereby offering a good platform for early clinical analysis.

Keywords Electrochemical immunosensor · Thionine · Label-free · Binary nanoparticle-decorated reduced graphene oxide-tetraethylene pentamine · Carcinoembryonic antigen

Introduction

Cancer has the highest mortality rate and is the most widely spread incurable disease. An effective way to treat and control cancer is through early diagnosis [1]. In clinical trials, serum cancer markers have been shown to be elevated in some cancer patients. The presence or quantitative changes in these tumor markers can reflect the nature of the tumor, thereby enabling the diagnosis, classification, treatment guidance, and prognosis of the tumor. Among them, CEA is the most common marker, which can be used for the clinical diagnosis of liver cancer, gastric cancer, pancreatic cancer, and other tumors [2]. A rapid and sensitive test to determine the concentration of CEA was vital for effective early prediction and diagnosis of cancer. Hence, a simple, efficient, accurate, and single-use point-of-care testing equipment for CEA measurement is urgently needed for early clinical diagnosis.

Immunoassay is a common method for clinical testing and biochemical analysis due to its high specificity and sensitivity [3–7]. For analysis and detection of tumor markers, many methods have been proposed, such as colorimetric immunoassay [8, 9], fluoroimmunoassay, enzyme-linked immunosorbent assay (ELISA) [10], and chemiluminescent immunoassay [11, 12]. However, the above methods have many limitations, such as the need for a large number of reagent kits and plant readers, complex and expensive machines, and professional technologists, which make these methods expensive and time-consuming. Therefore, alternative methods are needed to overcome these shortcomings. Of late, electrochemical immunoassay has received considerable attention because it is time-intensive, easy to operate, and inexpensive [1, 3–5]. Therefore, an excellent sensitive and biocompatible

✉ Zhencheng Chen
  chenzhcheng@163.com

✉ Liangli Cao
  caoliangli216@163.com

[1] School of Electronic Engineering and Automation, Guilin University of Electronic Technology, Guilin 541004, Guangxi, China

[2] School of Life and Environmental Sciences, Guilin University of Electronic Technology, Guilin 541004, Guangxi, China

[3] School of Information and Communication, Guilin University of Electronic Technology, Guilin 541004, China

electrochemical immunoassay for the determination of low concentrations of CEA in complex biological samples is essential for effective early cancer treatment.

Recently, some highly sensitive and selective sandwich-type immunosensors have been studied [13, 14]. However, the labeling process was complex and time-consuming, which reduced the stability and repeatability of the sensor. However, a label-free immunosensor could overcome the shortcomings of probe labeling and electrochemical index selection of sandwich-type immunosensors without reducing its sensitivity and selectivity. Therefore, it had solved an important concern of researchers and was considered a promising test method [7–9].

Due to the good electrical conductivity and good biocompatibility of nanomaterials, they were often used to modify immunosensors to immobilize antibodies and amplify signals [10]. Graphene is a well-known material composed of a single layer of carbon atoms. It is a two-dimensional material with only one carbon atom thickness, composed of sp^2-hybridized carbon atoms arranged in a hexagonal honeycomb lattice [15]. Graphene oxide (GO) is a graphene sheet decorated with abundant oxygen-containing functional groups, such as hydroxyl groups (-OH) and carboxyl groups (-COOH) [16]. However, the conductivity of GO is less due to many defects that exist in its structure. Chemical reduction can restore the conductivity of GO by removal of oxygen. Due to the high electrochemical activity of reduced graphene oxide (rGO), it is often used in electrochemical sensors. However, the aggregation of rGO affects the performance of electrochemical immunosensors [11]. Therefore, it is necessary to improve the stability of rGO by covalent functionalization. For example, covalent functionalization of rGO with tetraethylene pentamine (TEPA) produces the amino-functionalized rGO-TEPA [12]. It not only significantly increases the specific area of rGO but also ameliorates its dispersibility. Therefore, rGO-TEPA is an ideal substrate material for electrode modification [12, 17]. Iron-oxide magnetic nanoparticles (MNPs) were selected to modify rGO-TEPA to prevent further agglomeration because of their unique physicochemical properties, including large surface area, rapid diffusion, and excellent dispersion. Besides, when performing solid-liquid phase separation, magnetic separation can be applied for the purification of biomolecules, such as enzymes, proteins, and nucleic acids, because it was more convenient and rapid than conventional separation techniques, such as centrifugation or filtration [18, 19]. Gold nanoparticles (AuNPs) were used to immobilize antibodies and amplify signals because of their good biocompatibility, good conductivity, and large surface-to-volume ratio [20]. Most immunosensors require some media or labeled antigen or antibody to reflect the amount of bound antigen or antibody [12, 21–23]. Thi, a type of cationic phenothiazine dye, is used as an electrical signal indicator in electrochemical detection [24]. Thus, rGO-TEPA, MNPs, AuNPs, and Thi were used to build an immunosensing platform.

In this study, a new electrochemical immunosensor was prepared based on Au/MNPs-rGO-TEPA nanomaterials and was used to detect CEA. MNPs and AuNPs co-modified rGO-TEPA were used to improve water solubility of the substrate material and enhance the electrochemical signals. Thi molecule was used as an electrochemical indicator, which could adsorb on rGO-TEPA. Based on this characteristic, an Au/MNPs-rGO-TEPA/Thi-based immunosensor was successfully constructed for the detection of CEA. The proposed method indicated that the immunosensor had potential applications in early clinical analysis.

Experimental

Reagents and Materials

rGO-TEPA was purchased from Xianfeng Nano Materials Tech Co. Ltd. (Nanjing, China). Thi was purchased from Shanghai Yuanye Bio-Technology Co. Ltd. Gallic acid monohydrate (GA; 3, 4, 5-trihydroxy benzoic acid monohydrate) was purchased from Aladdin Inc. (Shanghai China). $FeCl_3$, $FeCl_2 \cdot 4H_2O$, NH_3OH, NaH_2PO_4, and Na_2HPO_4 were ordered from XiLong Chemical Co. Ltd. (Shanghai, China). Bovine serum albumin (97%, BSA) and hydrogen tetrachloroaurate (99%, $HAuCl_4 \cdot 4H_2O$) were purchased from Sigma-Aldrich (St. Louis, MO, USA). CEA and anti-CEA were ordered from Shanghai Linc-Bio Science Co. Ltd. (Shanghai, China). The other chemical reagents are of analytical grade. Distilled water was used in all the experiments.

Apparatus

The prepared nanocomposite was centrifuged using a medical centrifuge (TGL-20M, Hunan Xiangyi, China). rGO-TEPA, GA-modified MNPs (GA-MNPs), and the Au/MNPs-rGO-TEPA were analyzed by using transmission electron microscopy (TEM, Tokyo, Japan) and X-ray energy dispersive spectroscopy (EDS, Tokyo, Japan). UV-vis spectra were obtained by using a UH5300 UV-visible spectrophotometer (Perkin-Elmer, USA). Fourier-transform infrared spectra (FT-IR) were collected by using a Nicolet 6700 FT-IR spectrometer (Shanghai Lerui Scientific Instrument, China). The X-ray diffraction (XRD) analyses were performed using a powder X-ray diffractometer (Tokyo, Japan). Differential pulse voltammetry (DPV), cyclic voltammetry (CV), and electrochemical impedance spectroscopy (EIS) were performed on a CHI660E electrochemical workstation (Shanghai Chenhua Instrument, China) using a carbon electrode as the counter electrode, Ag/AgCl electrode as the reference electrode, and another carbon electrode as the working electrode.

Scheme 1 Preparation process of the Au/MNPs-rGO-TEPA/Thi-based electrochemical immunosensor
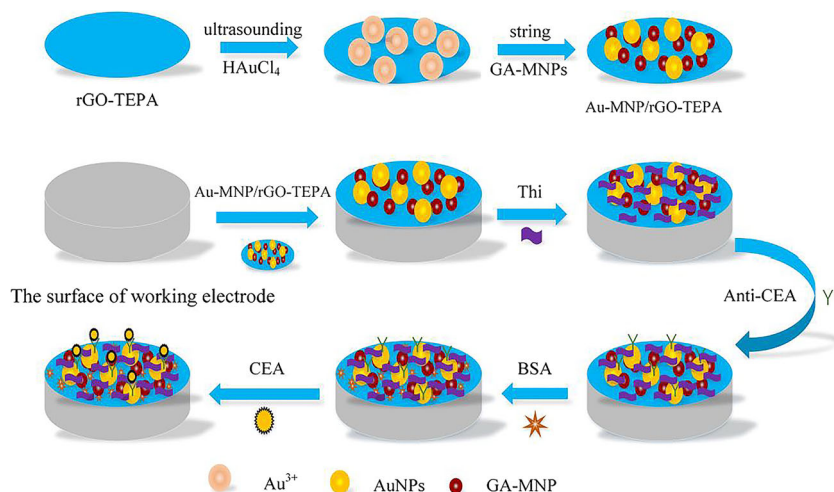
Synthesis of Au/MNPs-rGO-TEPA/Thi Nanocomposite

Au/MNPs-rGO-TEPA was prepared according to Lee's method [25], but with a minor modification. Briefly, 2 mmol $FeCl_3$ and 1 mmol $FeCl_2 \cdot 4H_2O$ were dissolved in deionized (DI) water. Then, 1 mL of NH_4OH (25% w/w) was poured into

this mixture. The resulting solution was stirred for 10 min, till it turned black. Subsequently, 3 mmol GA powder was mixed with this black magnetic solution and stirred in an oil pot at 90 °C for 30 min. The black solution turns dark violet, indicating the formation of GA-MNPs. Afterwards, the GA-MNPs were washed and separated. Next, an aqueous solution

Fig. 1 TEM images: **a** rGO-TEPA, **b** GA-MNPs, **c** Au/MNPs-rGO-TEPA (low magnification), and **d** Au/MNPs-rGO-TEPA (high magnification)
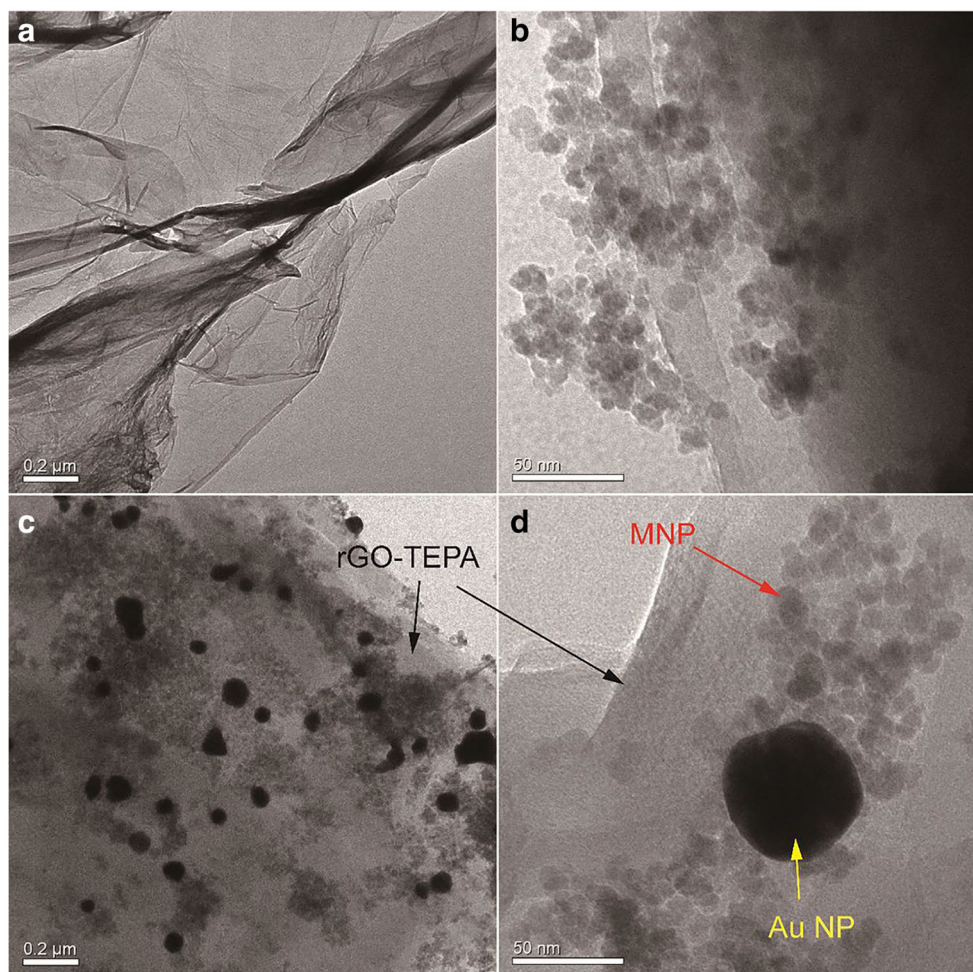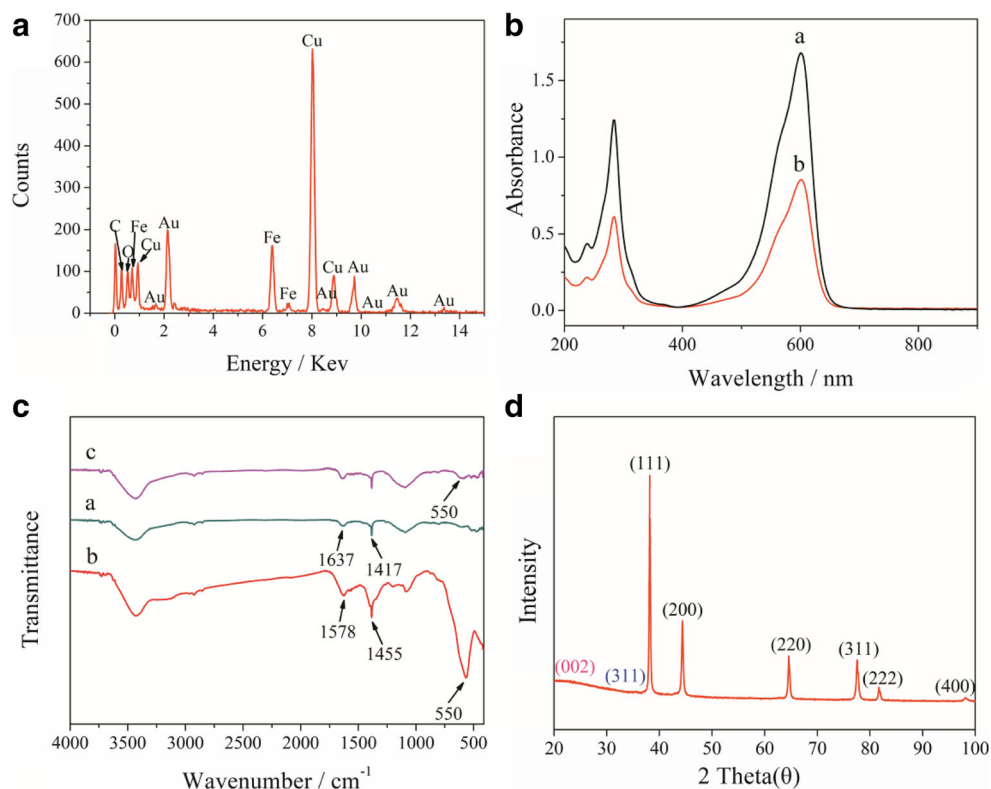
Fig. 2 **a** EDS image of Au/MNPs-rGO-TEPA. **b** UV-vis absorption spectra of (a) Thi and (b) Au/MNPs-rGO-TEPA/Thi. **c** FTIR spectrum of (a) rGO-TEPA, (b) GA-MNPs, and (c) Au/MNPs-rGO-TEPA. **d** XRD pattern (red, rGO-TEPA; blue, GA-MNPs; and black, AuNPs) of Au/MNPs-rGO-TEPA

(40 mL) containing rGO-TEPA (5 mg) and $HAuCl_4 \cdot 4H_2O$ (10 mmol) was poured into a beaker for 30 min with ultrasonication, and then 1 mL of GA-MNPs solution was poured into the as-prepared suspension with stirring. After 3 h, the black mixture turned dark red, indicating the successful preparation of Au/MNPs-rGO-TEPA. The as-prepared nanocomposites were magnetically separated and redispersed in 2 mL DI water. Finally, the as-prepared Au/MNPs-rGO-TEPA suspension was mixed with Thi solution (2 mg/mL) and stirred vigorously for 24 h. The resulting products were centrifuged and washed to remove some of the free Thi molecules.

Preparation of Immunosensor

Scheme 1 outlines the stepwise preparation of the Au/MNPs-rGO-TEPA/Thi-based sensor. First, 10 mL of the Au/MNPs-rGO-TEPA/Thi suspension was dripped on screen-printed electrode (SPE) and dried. Next, 10 μL of anti-CEA was dropped onto the working electrode and incubated in a refrigerator. After washing with PBS, the immunosensor was prepared by blocking the non-specific adsorption sites with BSA and then stored in the refrigerator at 4 °C without using.

Electrochemical Measurements

The prepared immunosensor was incubated with different concentrations of CEA for 30 min. After the uncombined antigen

was carefully washed away using 0.01 M PBS (pH 7.4), the CV measurements were performed in 0.01 M PBS with a scanning voltage ranging from − 0.8 to 0.2 V at a scanning rate of 0.1 V/s. DPV measurements were conducted in a voltage range from − 0.7 to 0.1 V, pulse amplitude of 50 mV, pulse width of 50 ms, and pulse period of 1 s. EIS was performed in a 5 mM $[Fe(CN)_6]^{3-/4-}$ solution with a frequency range from 10^{-1} to 10^5 Hz and an initial voltage of 0.24 V.

Results and Discussion

Characterization of Au/MNPs-rGO-TEPA Nanocomposite

As shown in Fig. 1, the morphology and size of rGO-TEPA, GA-MNPs, and the Au/MNPs-rGO-TEPA nanocomposite were characterized by TEM. Fig. 1a shows that rGO-TEPA has a paper-like morphology with high surface-to-volume ratio suitable for electron transfer. Many small gray particles were distributed on the GA (Fig. 1b), indicating that GA-MNPs were successfully prepared. Two different nanoparticles were observed on the rGO-TEPA surface (Fig. 1c, d): the large black spots were AuNPs, whereas the small gray particles were MNPs. This result illustrated that the MNPs and AuNPs were successfully adsorbed on rGO-TEPA. The EDS results of Au/MNPs-rGO-TEPA (Fig. 2a) also confirmed the existence of Au and Fe in the Au/MNPs-rGO-TEPA.
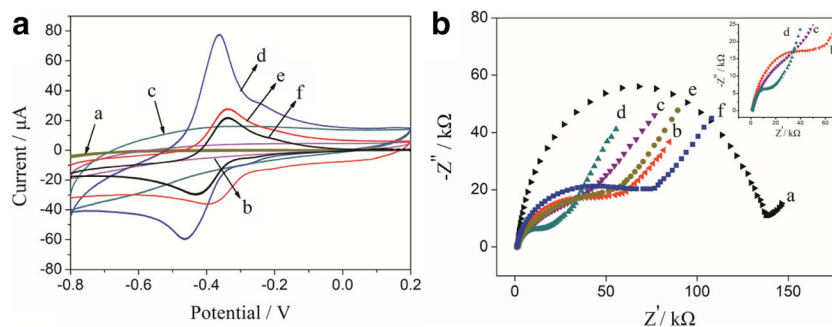
Fig. 3 a CV curves of the different electrodes: (a) bare SPE, (b) rGO-TEPA/SPE, (c) Au/MNPs-rGO-TEPA/SPE, (d) Au/MNPs-rGO-TEPA/Thi/SPE, (e) Au/MNPs-rGO-TEPA/Thi/anti-CEA/SPE, and (f) Au/MNPs-rGO-TEPA/Thi/anti-CEA/BSA/SPE in the 0.01 M pH 7.0 PBS solution. **b** EIS curves of the different electrodes: (a) bare SPE, (b) rGO-TEPA/SPE, (c) Au/MNPs-rGO-TEPA/SPE, (d) Au/MNPs-rGO-TEPA/Thi/SPE, (e) Au/MNPs-rGO-TEPA/Thi/anti-CEA/SPE, and (f) Au/MNPs-rGO-TEPA/Thi/anti-CEA/BSA/SPE in the 0.01 M pH 7.4 PBS and 5.0 mM $[Fe(CN)_6]^{3-/4-}$ solution

The UV-visible absorption spectra of Thi and rGO-TEPA are shown in Fig. 2b. Absorption by the C=N bond resulted in a red shift from 600 to 602 nm, and the absorption by aromatic hydrocarbons produced a blue shift from 283 to 280 nm. This indicated that the Thi molecules were immobilized onto Au-MNPs/rGO-TEPA via π-π stacking interaction between Thi molecules and rGO-TEPA [26].

As shown in Fig. 2c, the functional groups of rGO-TEPA, GA-MNPs, and Au/MNPs-rGO-TEPA were analyzed by using FITR spectroscopy. In the FTIR spectrums of the GA-MNPs (curve b) and Au/MNPs-rGO-TEPA (curve c), the characteristic peak of Fe-O at 550 cm^{-1} appears and the characteristic peak at 1578 cm^{-1} testifies the existence of the C=O vibration [27]. The N-H vibration (1637 cm^{-1}) and C-N vibration (1417 cm^{-1}) peaks were also observed for rGO-TEPA (curve a), which corresponded to the vibration spectrum of the Au/MNPs-rGO-TEPA (curve c). These results showed that Au/MNPs-rGO-TEPA was successfully prepared.

Fig. 2d shows the XRD patterns of Au/MNPs-rGO-TEPA. The (002; red) plane of rGO-TEPA appeared at $2\theta = 24.38°$ (ICSD card number: 01-075-1621), which was consistent with earlier reports [17]. The (311; blue) plane of the GA-MNPs (ICSD card number: 79-0417) was observed at $2\theta = 35.63°$ [25]. There were several characteristic peaks at $2\theta = 38.72°$, 44.35°, 64.73°, 77.45°, 81.83°, and 98.34°, corresponding to (111), (200), (220), (311), (222), and (400) planes of AuNPs,

respectively, indicating that AuNPs and MNPs had been successfully loaded onto the surface of rGO-TEPA.

Electrochemical Characteristics of the Immunosensor

The electrochemical responses of the modified SPE at different stages were studied by using CV and EIS for evaluating the performance of the proposed immunosensor. As shown in Fig. 3a, the CV responses of bare SPE, rGO-TEPA, Au/MNPs-rGO-TEPA, Au/MNPs-rGO-TEPA/Thi, Au/MNPs-rGO-TEPA/Thi/anti-CEA, and Au/MNPs-rGO- TEPA/Thi/anti-CEA/BSA modified SPEs were monitored in 0.01 M PBS (pH 7.4). No redox peak was observed in curves a, b, and c; however, the response currents of curves b and c gradually increased because the modification of rGO-TEPA and AuNPs on SPE enhanced the electron transfer rate. When SPE was modified with Au/MNPs-rGO-TEPA/Thi, a pair of symmetric redox peaks were observed at − 0.362 V and − 0.467 V (curve d), which were characteristic of Thi and could be used as suitable indicators for electrochemical detection. After being incubated with anti-CEA (curve e), the response current decreased significantly because anti-CEA was successfully immobilized on SPEs. When the immunosensor was blocked with BSA (curve f), the peak current decreased further because the deposited BSA hindered electron transfer.

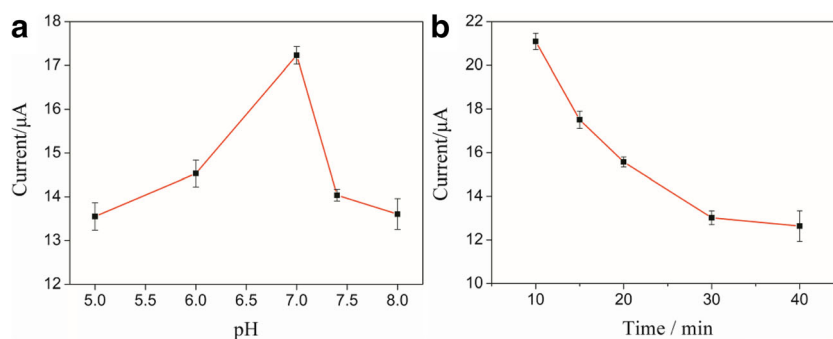**Fig. 4** Effects of **a** pH of detection solution and **b** incubation time on the immunosensor
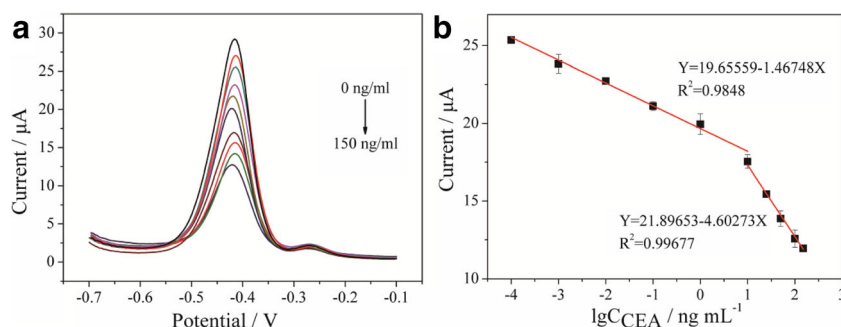
Fig. 5 DPV curves (**a**) and calibration curves (**b**) of the immunosensor incubated with different concentrations of CEA (0–150 ng/mL)

EIS is a common method for detecting the characteristics of immune complex decorated electrodes [24, 28, 29]. Fig. 3b shows the Nyquist plots obtained for the bare SPE (curve a), rGO-TEPA (curve b), Au/MNPs-rGO-TEPA (curve c), Au/MNPs-rGO-TEPA/Thi (curve d), Au/MNPs-rGO-TEPA/Thi/anti-CEA (curve e), and Au/MNPs-rGO-TEPA/Thi/anti-CEA/BSA(curve f) in the presence of 5 mM $[Fe(CN)_6]^{3-/4-}$ solution. Each of the impedance spectrum has two portions. The straight line partly corresponds to the diffusion process of the system, and the semicircular portion corresponds to the electron transfer resistance (R_{et}), where the electron transfer impedance is equal to the diameter of the semicircle. As shown in Fig. 3b, a large resistance (curve a) was observed, which corresponded to the bare SPE. When rGO-TEPA modified onto the electrode, its resistance decreased significantly (curve b). This indicated that rGO-TEPA has good electroactivity, which promoted electron transfer. When AuNPs and MNPs were adsorbed on the materials, a slightly smaller resistance (curve c) was observed, which was due to AuNPs and MNPs further facilitating electron transfer. The resistance decreased to a minimum after Thi was modified on Au/MNPs-rGO-TEPA/SPE (curve d). The resistance increased after anti-CEA and BSA were successively adsorbed onto the modified electrode because the protein molecules hindered the electron transfer. It indicated that the immunosensor was successfully modified layer by layer.

Optimization of Analytical Condition

The optimal conditions of the immunosensor include incubation time and pH. DPV was used to detect the optimal conditions in 0.01 M PBS. Fig. 4 shows the effects of pH of substrate solution (Fig. 4a) and incubation time (Fig. 4b) on the DPV response to 1 ng/mL CEA solution. Since Thi can generate electrochemical signals in acidic environment and the proposed immunosensor was based on Thi to display the electrochemical signal, it is important to optimize the pH of the reaction solution. To test the influence of solution pH, it was tested in PBS with pH ranging from 5.0 to 8.0 and used to detect 1 ng/mL of CEA solution. In the pH range 5.0–7.0, the response current increased with increasing pH and decreased when the pH exceeded 7.0 (Fig. 4a). Experiments have shown that over-acidic or over-alkaline conditions can damage the immunosensor. Therefore, pH 7.0 is selected as the optimum pH for all the electrochemical tests.

Incubation time also affected the electrochemical reaction. To test the influence of incubation time, the modified electrodes were immersed in 1 ng/mL CEA for different periods (10, 15, 20, 30, and 40 min) (Fig. 4b). With increasing incubation time, the peak current decreased rapidly and gradually stabilized after 30 min. Therefore, 30 min was chosen as the experimental incubation time.

Table 1 Comparison of the previously reported CEA sensor and the proposed immunosensor

| Detection method	Linear range	Detection limit	References
Electrochemical immunosensor	0.0001–20 ng/mL	0.03 pg/mL	[30]
Sandwich aptasensor	5–40 ng/mL	3.4 ng/mL	[31]
Electrochemical immunosensor	0.05–0.5 μg/mL	0.035 μg/mL	[32]
Electrochemical immunosensor	0.1–750 ng/mL	90 pg/mL	[33]
Fluorescence method	1–100 ng/mL	0.049 ng/mL	[34]
Electrochemical immunosensor	0.1–1000 ng/mL	0.007 ng/mL	[35]
Colorimetric aptasensor	1–50 ng/mL	1 ng/mL	[36]
Electrochemiluminescence immunosensor	0.005–500 ng/mL	1.67 pg/mL	[14]
Electrochemical immunosensor	0.0001–1 ng/mL and 1–150 ng/mL	0.06 pg/mL	This work
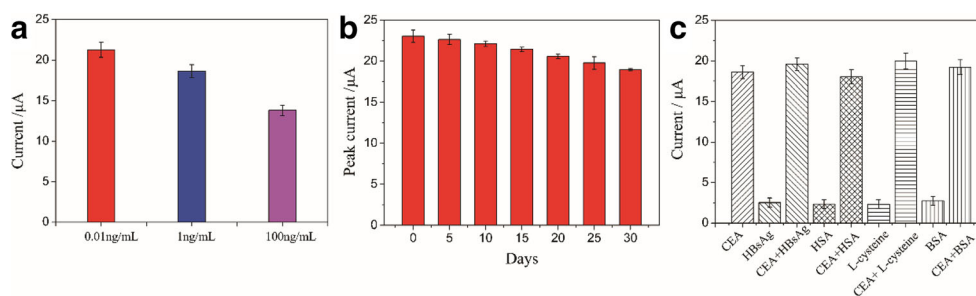
Fig. 6 **a** Electrocatalytic current responses of different batches of immunosensor to 0.01 ng/mL, 1 ng/mL, and 100 ng/mL of CEA. **b** The stability studies of immunosensor (error bar = RSD, $n = 5$). **c** Amperometric response of the immunosensor to 1 ng/mL CEA, 100 ng/ mL HBsAg, 1 ng/mL CEA + 100 ng/mL HBsAg, 100 ng/mL HSA, 1 ng/ mL CEA + 100 ng/mL HSA, 100 ng/mL L-cysteine, 1 ng/mL CEA + 100 ng/mL L-cysteine, 100 ng/mL BSA, 1 ng/mL CEA + 100 ng/mL BSA

Analytical Performance of the Immunosensor

To evaluate the performance of the proposed immunosensor, different concentrations of CEA solutions were determined under the above-mentioned optimized conditions. Fig. 5a shows the obtained DPV response for applied voltages ranging from − 0.7 to − 0.1 V. The peak current at − 0.42 V appears due to the reduction of the oxidation products of Thi, which decreased as the concentration of CEA increased from 0.1 pg/mL to 150 ng/ mL (Fig. 5b). The linear regression equation, in the CEA concentration range from 0.1 pg/mL to 1 ng/mL, was $I = 19.65559 – 1.46748 \times lgC_{CEA}$, with a correlation coefficient of 0.9848, and in the CEA concentration range from 1 ng/mL to 150 ng/mL, was $I = 21.89653 – 4.60273 \times lgC_{CEA}$, with a correlation coefficient of 0.99677. On the basis of triple standard deviation, the LOD was calculated to be 0.06 pg/mL.

Table 1 shows the comparison of the linear range and LOD of the proposed method with those of some previously published CEA sensors. The results reveal that the prepared immunosensor had better detection limit and wider linear range.

Reproducibility, Stability, and Specificity of the Immunosensor

Three different concentrations of CEA (10 pg/mL, 1 ng/mL, and 100 ng/mL) were detected by using DPV measurement. As displayed in Fig. 6a, the relative standard deviation (RSD) of the measurements was 2.1%, indicating that the immunosensor has good reproducibility. The immunosensor

was stored for 30 days at 4 °C and measured every 5 days. As shown in Fig. 6b, the immunosensor maintained ~ 82% of its initial current signal after 1 month, which indicated that the sensor can maintain its bioactivity and stability for up 30 days. Hepatitis B surface antigen (HBsAg), human serum albumin (HSA), L-cysteine, BSA, and CEA (100 ng/mL each) were chosen as the interfering substances for assessing the specificity of the immunosensor (Fig. 6c). Compared with immunosensors containing interfering substances, the peak value of the response current obtained by DPV measurements was not significantly different. Therefore, the specificity of the immunosensor was excellent.

Real Sample Analysis

To evaluate the reliability of the constructed immunosensor, three different clinical blood samples were tested. Results obtained from standard electrochemiluminescence (ECL) immunoassay were compared with the results obtained by using our proposed immunosensor. Table 2 shows that the relative errors were in the range from − 3.61% to 1.04%, suggesting that the developed immunosensor can be used as a quick and accurate tool for the detection of CEA in human blood samples.

Conclusion

In this study, Au/MNPs-rGO-TEPA/Thi composites were successfully synthesized and used to construct a sensitive

Table 2 Detection of CEA in human serum samples with the as-constructed immunosensor

Sample	Reference method (ng/mL)[a]	Proposed method (ng/mL)[b]	Relative error (%)
1	2.40	2.49 ± 0.09	− 3.61
2	36.60	36.22 ± 1.12	15
3	95.20	92.56 ± 2.96	2.85

[a] The results of the reference were provided by the 924 Hospital of the People's Liberation Army Joint Service Support Force were tested through electrochemical luminescence

[b] Results and relative errors obtained by testing each sample five times

electrochemical immunosensor for rapid analysis of low concentrations of CEA. The as-prepared Au/MNPs-rGO-TEPA/Thi nanocomposites not only increased the adsorbing capacity of anti-CEA but also retained the electrochemical activity of Thi. Under optimal conditions, the proposed immunosensors showed good sensitivity over a wide linear range (from 0.1 pg/mL to 150 ng/mL) and a low detection limit of 0.06 pg/mL. Furthermore, the proposed immunoassay method showed acceptable stability, reproducibility, and specificity, providing a method for the detection of some other biomarkers in clinical analysis.

Compliance with Ethical Standards

Conflict of Interest   The authors declare that they have no conflict of interest.

References

1. M.A. Mohammad, T.A. Zahra, N. Sahraei, S.M. Moshtaghioun, Biosens. Bioelectron. **129**, 1–6 (2019)
2. J.J. Miao, X.B. Wang, L.D. Lu, P.Y. Zhu, C. Mao, H. Zhao, Y. Song, J. Shen, Electrochemical immunosensor based on hyperbranched structure for carcinoembryonic antigen detection. Biosens. Bioelectron. **58**, 9–16 (2014)
3. Y. Zhang, M.Y. Li, X.M. Gao, Y. Chen, T. Liu, J. Hematol, Oncol. **12**, 137–137 (2019)
4. K. Njoku, D. Chiasserini, A.D. Whetton, E.J. Crosbie, Proteomic biomarkers for the detection of endometrial cancer. Cancers **11**(10), 1572 (2019)
5. K. Honda, M. Ono, M. Shitashige, M. Masuda, M. Kamita, N. Miura, T. Yamada, Proteomic approaches to the discovery of cancer biomarkers for early detection and personalized medicine. Jpn. J. Clin. Oncol. **43**(2), 103–109 (2013)
6. Y. Wang, J.P. Luo, J.T. Liu, X.R. Li, Z. Kong, H. Jin, X. Cai, Electrochemical integrated paper-based immunosensor modified with multi-walled carbon nanotubes nanocomposites for point-of-care testing of 17β-estradiol. Biosens. Bioelectron. **107**, 47–53 (2018)
7. Y. Wang, H.R. Xu, J.P. Luo, J.T. Liu, L. Wang, Y. Fan, S. Yan, Y. Yang, X. Cai, A novel label-free microfluidic paper-based immunosensor for highly sensitive electrochemical detection of carcinoembryonic antigen. Biosens. Bioelectron. **83**, 319–326 (2016)
8. F. Ahour, A. Shamsi, Electrochemical label-free and sensitive nanobiosensing of DNA hybridization by graphene oxide modified pencil graphite electrode. Anal. Biochem. **532**, 64–71 (2017)
9. M.A. Tabrizi, M. Shamsipur, R. Saber, S. Sarkar, Simultaneous determination of CYC and VEGF165 tumor markers based on immobilization of flavin adenine dinucleotide and thionine as probes on reduced graphene oxide-poly(amidoamine)/gold nanocomposite

10. modified dual working screen-printed electrode. Sens. Actuators B Chem. **240**, 1174–1181 (2017)
10. Y. Fan, S.Y. Shi, J.S. Ma, Y.H. Guo, A paper-based electrochemical immunosensor with reduced graphene oxide/thionine/gold nanoparticles nanocomposites modification for the detection of cancer antigen 125. Biosens. Bioelectron. **135**, 1–7 (2019)
11. J.M. Han, J. Ma, Z.F. Ma, One-step synthesis of graphene oxide–thionine–Au nanocomposites and its application for electrochemical immunosensing. Biosens. Bioelectron. **47**, 243–247 (2013)
12. D. Wu, A.P. Guo, Z.K. Guo, L.L. Xie, Q. Wei, B. Du, Simultaneous electrochemical detection of cervical cancer markers using reduced graphene oxide-tetraethylene pentamine as electrode materials and distinguishable redox probes as labels. Biosens. Bioelectron. **54**, 634–639 (2014)
13. Y.G. Wang, G.H. Zhao, Y. Zhang, X.H. Pang, W. Cao, B. Du, Q. Wei, Sandwich-type electrochemical immunosensor for CEA detection based on Ag/MoS2@Fe3O4 and an analogous ELISA method with total internal reflection microscopy. Sens. Actuators B Chem. **266**, 561–569 (2018)
14. N.L. Li, L.P. Jia, R.N. Ma, W.L. Jia, Y. Lu, S. Shi, H. Wang, A novel sandwiched electrochemiluminescence immunosensor for the detection of carcinoembryonic antigen based on carbon quantum dots and signal amplification. Biosens. Bioelectron. **89**(Pt 1), 453–460 (2017)
15. H. Wang, X.Z. Yuan, Y. Wu, H.J. Huang, X. Peng, G.M. Zeng, H. Zhong, J. Liang, M. Ren, Adv. Colloid Interf. Sci. **195**, 19–40 (2013)
16. J.J. Shao, W. Lv, Q.H. Yang, Self-assembly of graphene oxide at interfaces. Adv. Mater. **26**(32), 5586–5612 (2014)
17. S.Q. Yu, G.Z. Zou, Q. Wei, Talanta **156**, 11–17 (2016)
18. G. Aygar, M. Kaya, N. Ozkan, S. Kocabiyik, M. Volkan, J. Phys, Preparation of silica coated cobalt ferrite magnetic nanoparticles for the purification of histidine-tagged proteins. Chem. Solids **87**, 64–71 (2015)
19. Y.J. Liu, Y.Z. Wang, Q.Z. Dai, Y. Zhou, Magnetic deep eutectic solvents molecularly imprinted polymers for the selective recognition and separation of protein. Anal. Chim. Acta **936**, 168–178 (2016)
20. Y. Luo, F.Y. Kong, C. Li, J.J. Shi, W. Lv, W. Wang, One-pot preparation of reduced graphene oxide-carbon nanotube decorated with Au nanoparticles based on protein for non-enzymatic electrochemical sensing of glucose. Sens. Actuators B Chem. **234**, 625–632 (2016)
21. H.M. Ma, X.Y. Zhang, X.J. Li, R.X. Li, B. Du, Q. Wei, Electrochemical immunosensor for detecting typical bladder cancer biomarker based on reduced graphene oxide–tetraethylene pentamine and trimetallic AuPdPt nanoparticles. Talanta **143**, 77–82 (2015)
22. Z.L. Tan, L.L. Cao, Y.Y. Yang, Q. Yan, Q. Liu, W. Zhang, P. Zhao, Y. Li, D. Zhang, Amperometric immunoassay for the carcinoembryonic antigen by using a peroxidase mimic consisting of palladium nanospheres functionalized with glutathione-capped gold nanoparticles on graphene oxide. Microchim. Acta **186**(11), 693 (2019)
23. Z. Savari, S. Soltanian, A. Noorbakhsh, A. Salimi, M. Najafi, P. Servati, High sensitivity amperometric and voltammetric determination of persulfate with neutral red/nickel oxide nanowires modified carbon paste electrodes. Sens. Actuators B Chem. **176**, 335–343 (2013)
24. K.Q. Jiang, D.X. Nie, Q.W. Huang, K. Fan, Z. Tang, Y. Wu, Z. Han, Thin-layer MoS2 and thionin composite-based electrochemical sensing platform for rapid and sensitive detection of zearalenone in human biofluids. Biosens. Bioelectron. **130**, 322–329 (2019)
25. J. Lee, M. Morita, K. Takemura, E.Y. Park, A multi-functional gold/iron-oxide nanoparticle-CNT hybrid nanomaterial as virus DNA sensing platform. Biosens. Bioelectron. **102**, 425–431 (2018)

26. Z. Zhao, H.D. Chen, L.N. Ma, D.J. Liu, Z. Wang, A label-free electrochemical impedance aptasensor for cylindrospermopsin detection based on thionine–graphene nanocomposites. Analyst 140(16), 5570–5577 (2015)

27. J. Lee, K. Takemura, C.N. Kato, T. Suzuki, E.Y. Park, Binary nanoparticle graphene hybrid structure-based highly sensitive biosensing platform for norovirus-like particle detection. ACS Appl. Mater. Interfaces 9(32), 27298–27304 (2017)

28. X. Wang, C.C. Chu, L. Shen, W.P. Deng, M. Yan, S. Ge, J. Yu, X. Song, An ultrasensitive electrochemical immunosensor based on the catalytical activity of MoS2-Au composite using Ag nanospheres as labels. Sens. Actuators B Chem. 206, 30–36 (2015)

29. S. Su, X.Y. Han, Z.W. Lu, W. Liu, D. Zhu, J. Chao, C. Fan, L. Wang, S. Song, L. Weng, L. Wang, Facile synthesis of a MoS2–Prussian blue nanocube nanohybrid-based electrochemical sensing platform for hydrogen peroxide and carcinoembryonic antigen detection. ACS Appl. Mater. Interfaces 9(14), 12773–12781 (2017)

30. R. Wang, J.J. Feng, Y.D. Xue, L. Wu, A. Wang, A label-free electrochemical immunosensor based on AgPt nanorings supported on reduced graphene oxide for ultrasensitive analysis of tumor marker. Sens. Actuators B Chem. 254, 1174–1181 (2018)

31. Q.L. Wang, H.F. Cui, X.J. Song, S.F. Fan, L. Chen, M. Li, Z. Li, A label-free and lectin-based sandwich aptasensor for detection of carcinoembryonic antigen. Sens. Actuators B Chem. 260, 48–54 (2018)

32. S.X. Lee, H.N. Lim, I. Ibrahim, A. Jamil, A. Pandikumar, N.M. Huang, Horseradish peroxidase-labeled silver/reduced graphene oxide thin film-modified screen-printed electrode for detection of carcinoembryonic antigen. Biosens. Bioelectron. 89(Pt 1), 673–680 (2017)

33. J.Y. Liu, J. Wang, T.S. Wang, D. Li, F. Xi, J. Wang, E. Wang, Three-dimensional electrochemical immunosensor for sensitive detection of carcinoembryonic antigen based on monolithic and macroporous graphene foam. Biosens. Bioelectron. 65, 281–286 (2015)

34. W.J. Qin, K. Wang, K. Xiao, Y.F. Hou, W. Lu, H. Xu, Y. Wo, S. Feng, D. Cui, Carcinoembryonic antigen detection with "Handing"-controlled fluorescence spectroscopy using a color matrix for point-of-care applications. Biosens. Bioelectron. 90, 508–515 (2017)

35. X.Q. Li, M.X. Yu, Z.C. Chen, X. Lin, Q. Wu, A sensor for detection of carcinoembryonic antigen based on the polyaniline-Au nanoparticles and gap-based interdigitated electrode. Sens. Actuators B Chem. 239, 874–882 (2017)

36. N. Shahbazi, S. Hosseinkhani, B. Ranjbar, A facile and rapid aptasensor based on split peroxidase DNAzyme for visual detection of carcinoembryonic antigen in saliva. Sens. Actuators B Chem. 253, 794–803 (2017)